Review

Cathode Materials for Intermediate Temperature Solid Oxide Fuel Cells

Jamila Nisar , Gurpreet Kaur , Sarbjit Giddey * , Suresh Bhargava , Lathe Jones

Posted Date: 13 May 2024

doi: 10.20944/preprints202405.0747.v1

Keywords: Solid oxide fuel cell; Cathode materials; Perovskites; Doping; Infiltration; Core-shell composite

Review

Cathode Materials for Intermediate Temperature Solid Oxide Fuel Cells

Jamila Nisar [1,2], Gurpreet Kaur [1], Sarbjit Giddey [1,*], Suresh Bhargava [2] and Lathe Jones [2]

[1] CSIRO Energy, Private Bag 10, Clayton South-3169, Victoria, Australia
[2] School of Science, RMIT University, Melbourne, Victoria, Australia
* Correspondence: Sarb.Giddey@csiro.au.

Abstract: Intermediate temperature solid oxide fuel cell (SOFC) operation provides numerous advantages such as high combined heat and power (CHP) efficiency, potentially long-term materials stability, and the use of low-cost materials. However, due to the sluggish kinetics of the oxygen reduction reaction at intermediate temperature, the cathode of SOFC requires an efficient and stable catalyst. Significant progress in the development of cathode materials has been made over recent years. In this article, multiple strategies for improving the performance of cathode materials have been extensively reviewed such as A and B site doping of perovskites, infiltration of catalytic active materials, the use of core-shell composites, etc. Emphasis has been given to intrinsic properties such as thermal expansion compatibility, chemical and thermal stability, and oxygen transport number. Furthermore, to avoid any insulating phase formation at the cathode/electrolyte interface, strategies for interfacial layer modifications have also been extensively reviewed and summarized. Based on major technical challenges, future research directions have been proposed for efficient and stable intermediate temperature solid oxide fuel cell (SOFC) operation.

Keywords: solid oxide fuel cell (SOFC); cathode materials; perovskites; doping; infiltration; Core-Shell composite

1. Introduction

1.1. Background

Fossil fuels have been the prime source of electricity generation since the mid-19th century with nuclear energy as the next major source. Electricity production from coal is the largest among fossil fuels worldwide, for instance in Australia alone, it produced 54 % out of the total 76% of the energy produced from coal in 2020 as shown in Figure 1 [1].

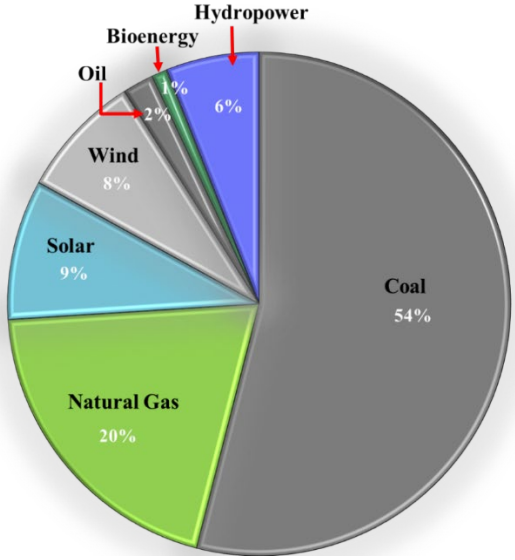

 doi:10.20944/preprints202405.0747.v1

Figure 1. Net Energy generation in 2020 by fuel type in Australia. Figure recreated from U.S Energy Information Administration with data from the Australian Department of Industry, Innovation, and Science [1].

Electricity production from coal emits harmful gases (CO_2, CH_4, SO_2 etc.) and other pollutants which significantly contributes to global warming and cause consequential health-related issues. The transition from fossil fuel energy to green renewable energy is the solution to improve air quality and reduce greenhouse gas emissions. Renewable energy capacity must meet the expectation of growing energy demand in addition to the competition of the well-established fossil fuel energy sector. A solid oxide fuel cell (SOFC) is one of the technologies being considered for efficient power generation with high-power generation efficiency up to 60-65% [2] and up to 80% with combined heat and power [3].

1.2. Fundamentals of SOFC

A fuel cell is an electrochemical device that generates electricity from the chemical energy of fuel in the presence of oxygen (from air). Fuel cells have three main cell components namely cathode, electrolyte, and anode. The schematic of the solid oxide fuel cell is represented in Figure 2.

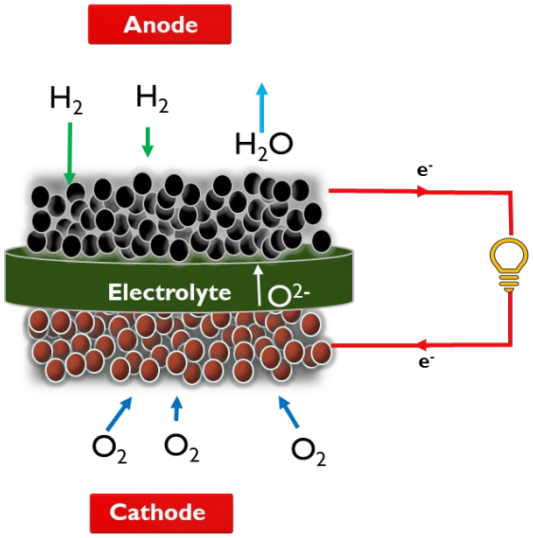

Figure 2. Schematic representation of SOFC based on oxide ion conducting (O-SOFC) electrolyte.

The oxygen supplied to the cathode is reduced to oxide anion by capturing electron at cathode/electrolyte interface (reaction 1). This oxygen anion then is transported through ceramic electrolyte to react with hydrogen supplied at the anode, resulting in the release of electrons and formation of water (reaction 2) and heat as the by-products. The electrons move through the external circuit and produce electricity. Each cell can generate an open circuit voltage (OCV) of about 1 V. Many cells can be stacked together to produce the required voltage / power for practical applications.

$$\tfrac{1}{2}\,O_2\,(g) + 2e^- \rightarrow O^{2-} \quad \text{(Cathode)} \quad (1)$$

$$O^{2-} + H_2(g) \rightarrow H_2O(g) + 2e^- \quad \text{(Anode)} \quad (2)$$

The overall reaction is

$$\tfrac{1}{2}\,O_2(g) + H_2\,(g) \rightarrow H_2O(g) \quad (3)$$

2. Materials and Requirements of Different Cell Components

2.1. Anode

Anode is the fuel electrode of the cell where oxidation of the fuel takes place. Anode should have high electronic conductivity (~100Scm^{-1}) and catalytic activity towards the oxidation of the fuels. In addition, anode should have thermal stability and chemical compatibility with other cell components.

 doi:10.20944/preprints202405.0747.v1

The most important regions where the reaction takes place is triple phase boundary (TPB) where fuel, electrolyte and anode come into contact.

Mixed ion electron conducting (MIEC) Ni-Yttria stabilized Zirconia (Ni/YSZ) composite is state of the art anode material and provide extended TPB sites from the electrode / electrolyte interface to the bulk of the electrode materials for efficient oxidation reaction of fuels. However, the major issue with this material is its degradation [4] with time (degradation rate of up to −0.094% per hour [5] or 0.014 mVh^{-1} [6]) due to Ni agglomeration changing Ni morphology in the matrix [7,8] and cross-reaction with interconnects [9].

2.2. Electrolyte

In SOFC the electrolyte is a ceramic membrane sandwiched between the air electrode and fuel electrode that conducts only ionic species through its lattice. The electrolyte is required to be dense and should have negligible electronic conductivity. Materials with oxide ion conductivity exceeding 0.01 Scm^{-1} and ionic transport number > 0.99 are typically used as an electrolyte in SOFC. Traditionally SOFCs are operated at high temperatures of 800 ℃-1000 ℃ to enable enough ionic transport through the electrolyte. For SOFC operation (above 800 ℃) the state of art oxygen ion-conducting electrolyte material is 8-10 mol% Yttria stabilized Zirconia (YSZ) which have good chemical stability and thermal expansion coefficient (TEC) compatibility with Ni/YSZ (anode) at operating temperature. At cathode/electrolyte interface, YSZ react with cathode materials ($LaMnO_3$) at high temperatures >900 °C [10] contributing to cell performance degradation.

The other prominent option for electrolyte include ceria-based electrolytes with high ionic conductivity like Gd doped ceria Gd-CeO_2 (GDC), Sm doped ceria Sm-CeO_2 (SDC) and $La_{1-x}Sr_xGa_{1-y}Mg_yO_3$ – (LSGM) [11]. However, thermal incompatibility with cathode due to a wide difference between the TEC values of doped ceria electrolytes (GDC = ~12.0×10^{-6} K^{-1} [12] and SDC = 12.6×10^{-6} K^{-1} at 800 ℃ [13]) and LSCF cathode material (15.6×10^{-6} K^{-1} at 700 ℃ [14] and 16.3×10^{-6} K^{-1} at 800 ℃ [15]) needs to be addressed.

2.3. Cathode

The cathode is oxygen electrode of the cell where oxygen reduction takes place. Like the anode, cathode material should have electrocatalytic activity, chemical compatibility with other components, thermal stability in cell operating conditions. The high operating temperature favours the faster oxygen reduction reaction (ORR) at the cathode which leads to achieve high power density of fuel cells. However, faster degradation rates, expensive cell components and more stringent requirements for sealings are the major drawbacks of high temperature cell operation. Reducing the temperature to 500 ℃ - 700 ℃ can potentially resolve some of these issues in addition to SOFC lifetime challenges. Some of the high and low temperature cell operation features are shown in Figure 3.

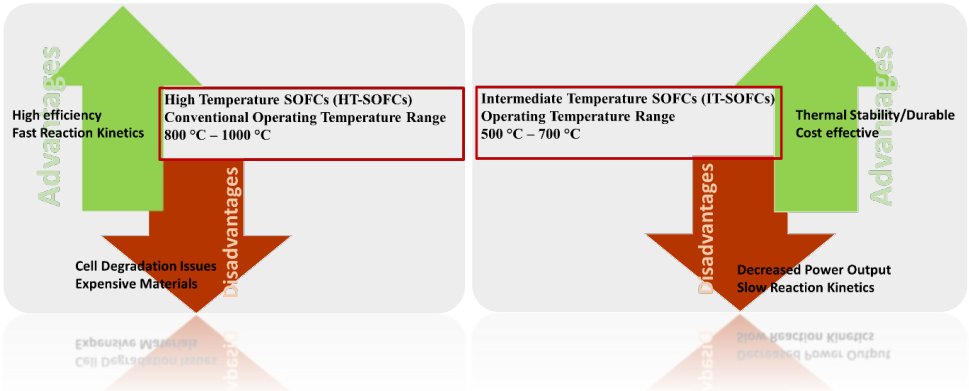

Figure 3. Comparison between Intermediate and High temperature SOFC.

Preprints.org (www.preprints.org) | NOT PEER-REVIEWED | Posted: 13 May 2024 doi:10.20944/preprints202405.0747.v1

At low temperature cell operations, major voltage losses are mainly due to slow reaction kinetics which leads to decrease in the performance of SOFC. In recent years, extensive R&D effort has been devoted to developing new efficient materials for intermediate temperature cell operations. This article not only has extensively reviewed the cathode materials but also covered and compiled in detailed the various strategies adopted to improve the kinetics of the existing materials in addition to future perspectives.

3. Strategies for Improvement in the Performance of Cathode Materials

3.1. Doping

Mixed ionic and electron conducting (MIEC) materials have been doped by many researchers to improve the electrochemical properties of the cathode materials for IT-SOFCs. Main examples of MIEC cathode material are $LaSrCoFeO_{3-\delta}$ (LSCF), $BaSrCoFeO_{3-\delta}$ (BSCF) and $SmCoO_{3-\delta}$ (SSC) etc. For solid oxide fuel cells and electrolysis applications, these materials can be used as anode and cathode based upon their electrochemical properties and redox stability [16–18].

Co based perovskites have been the materials of choice in many fields because of having mixed ionic and electron conductivity, thermal stability, and chemical compatibility with cell components. However, loss of Co from the lattice due to high temperature could trigger Co reduction [19]. To tackle physical and chemical stability issues, these perovskites have been incorporated with other metals either at A- site [20,21], B-site [22–24], and O-site (Table 1).

Effect on Structural Stability

The doping approach has been proved beneficial due to its abridged procedures with ease to harvest more oxygen vacancy concentrations for enhancing the oxygen flux through the material. Resistance of some of the LSCF based doped cathodes has been reported by Jia et al. [15].The sample doped with Bi^{+3} showed the highest electrocatalytic performance resulting in improved ORR due to the lone pair of electrons of Bi^{+3}. The comparatively small particle size of LBSCF (Bi-doped LSCF) resulted in extension of three phase boundary. The La^{+3} in Lanthanum cobalt ferities at A- site is often substituted with cations having similar ionic radii to apprehend structural stability [25].

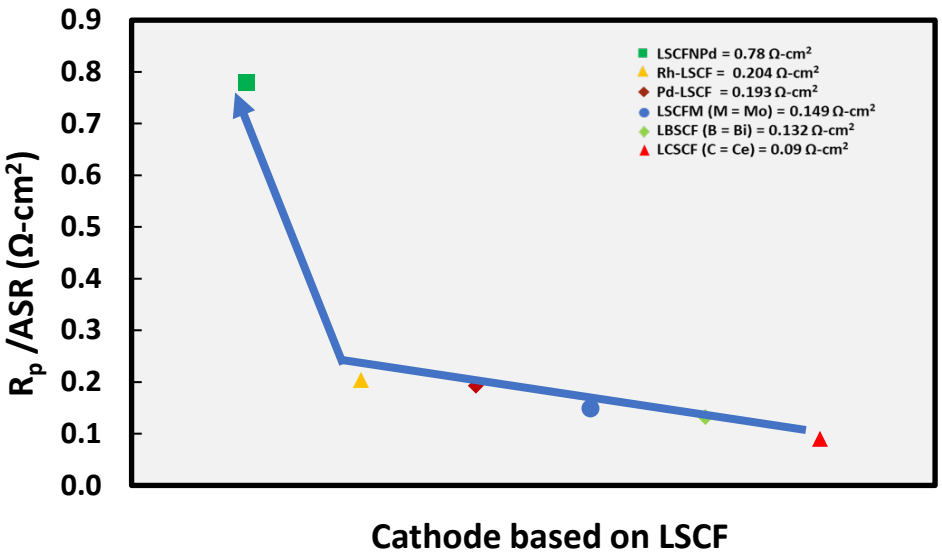

Figure 4. Resistance of LSCF based cathodes at 750 ℃. a) Nb and Pd doped LSCF (LSCFNPd) [26], b) Rh doped LSCF (Rh-LSCF) [27], c) Pd doped LSCF (Pd-LSCF) [27], d) Mo doped LSCF (LSCFM) [28], e) Bi doped LSCF (LBSCF) [15] and f) Ce doped LSCF (LCSCF) [25]. .

 doi:10.20944/preprints202405.0747.v1

Not only the thermal mismatch between cathode materials and electrolytes [11], the phase instability for example, phase transition from cubic to hexagonal phase in BSCF at high working temperature can impact the oxygen ion flux. Zhu et al. [27] reported the enhancement in the oxygen permeability as well as the enhanced electrocatalytic performance of the BSCF by optimizing the doping amount of the Ba in A- site of the perovskite. The study suggested the transition to hexagonal phase is more pronounced by increasing the Ba content in A-site due to difference in ionic radii of the Ba and Sr [29]. Weber et al. [30] reported that and Ti doping in B-site of BSCF reduced the formation of secondary phases by up to 95%. They argued that the reason for the phase stability is the existence of Co^{+2} which is triggered by high valency of dopant cations. The whole process eradicates hexagonal phase transition by controlling the CoO and other Co species, thus rendering stability to the system [30].

Effect on Conductivity

The enhanced performance of metal cation doped perovskites is attributed to mixed valance couple formation (Co^{+3}/Co^{+4} or Fe^{+2}/Fe^{+3}) and assists in the oxygen transport in cathode microstructure. Substituting or doping the smaller valence cations (larger ionic radius cations) than Co or Fe in the B-site leads to the increment in the lattice parameter creating higher amount of the oxygen vacancies in the lattice structure [31]. The effect of introduced stresses in the grains on the lattice dimensions of perovskites by doping has shown its effect on the electrical conductivity due to altering porosity of the cathode material [32]. However it has been observed that , with the similar grain size of perovskites with entirely different dopants the perovskite cathode material with more charge carrier concentration always showed higher conductivity, i.e., having more mixed valence cation concentration [24].

The larger number of vacancy formation is believed to reduce the electrical conductivity due to hindering the oxygen transport channel along crystal lattice through these vacant spaces. There are two theories related to the effect of the unit cell volume on the oxygen transport as some authors reported that increase in the unit cell volume have a positive effect on the oxygen transport by increasing the size of transport channel which facilitates the oxygen transport while others suggest smaller unit cell volume helps in the shortening of the distance between oxygen moieties which favours the oxygen transport [33].

Anbo et al. [20] attempted to find out the effect of the ionic radii of the rare earth metals in $Nd_{1-x}Ln_xBaCo_2O_{6-\delta}$ (Ln represents La = 1.032 A°, Sm = 0.958 A°, Gd =0.938 A° as compared to Nd = 0.938 A°) on the concentration of the oxygen vacancy and crystal structure. The $Nd_{0.9}La_{0.1}BaCo_2O_{6-\delta}$ was reported to have better electrochemical performance than other systems in terms of activation energy E_a, and polarization resistance Rp with larger ionic radius. The free oxygen volume facilitates the oxygen movement through the lattice structure by lowering the activation energy needed for oxygen transport. The free oxygen volume V_f is calculated by the expression.

$$V_f = a.\,b.\,c. - 0.75\pi\,(r^3(A_1) + r^3(A_2) + 2r^3(B)\,(6-\delta)\,r^3(O) \qquad (4)$$

(a,b,c represents the three lattice parameters of the system and $r(A_1)$, $r(A_2)$, r(B) and r(O) are ionic radii of A_1, A_2, metal cations and oxygen anion, respectively). Although the results supported the claims, but the high TEC value ($23\times10^{-6}\ K^{-1}$) of NdLaBaCoO questions the thermal compatibility with the electrolytes such as GDC and LSGM ($11 - 13.2\times10^{-6}\ K^{-1}$ at 800 °C [12,15]) and consequently the durability of the system [20].

Effect on Coefficient of Thermal Expansion (TEC)

Although metal cation substitution at A- site is helpful to increase the electronic conductivity and surface oxygen diffusivity, the TEC of the electrode material have been observed to be increased in many cases, for example, TEC increases with La content in $Pr_{2-x}La_xNi_{0.85}Cu_{0.1}Al_{0.05}O_{4-\delta}$, (PNCA) cathode material as reported by Zhou. Q et al. [34].

On the other hand, doping with high valence cations like Nb, Ti and Zr in B-site of the perovskite observed to improve the thermal compatibility issues. For example, TEC of Nb doped at B-site of BSCF is $18\times10^{-6}K^{-1}$ in comparison to non-doped BSCF ($21\times10^{-6}\ K^{-1}$) as reported by Huang,Y et al. [35].

 doi:10.20944/preprints202405.0747.v1

The lattice volume contraction caused by increased bond strength due to Nb^{+5} doping decreases the TEC value of the system.

Another emerging strategy to address the conductivity related issues and thermal mismatch simultaneously is O-Site substitution (refer to Table 1). This approach showed the positive impact on oxygen diffusion coefficient and on improving thermal expansion compatibility as observed in $PrBaCo_2O_{5+\delta}$ [36].

Doping fluorine in O-Site also maintained the tetragonal phase structure ($0.1<x<0.2$). The strengthening of bond between Co-F due to more electronegative and smaller 'F' than 'O' is helpful in controlling the Co reduction at higher temperatures. The substitution of O by F reduced TEC from 24.0×10^{-6} K^{-1} to 20.86×10^{-6} K^{-1} and 16.78×10^{-6} K^{-1} for x= 0.1 and x= 0.2, but further improvements are still required in comparison to TEC of SDC (12.6×10^{-6} K^{-1}) and YSZ (10.3×10^{-6} K^{-1}) at 800 ℃. Similar trend is observed in $BaCo_{0.4}Fe_{0.4}Zr_{0.1}Y_{0.1}O_{3-\delta}F$ by Wang et al. [37]. The cubic structure of $BaCo_{0.4}Fe_{0.4}Zr_{0.1}Y_{0.1}O_{3-\delta}F$ is stabilized by 'O' anion substitution. The more electronegative F^- ion helped in changing the lattice structure in cubic form as analysed by Raman spectroscopy. The effect of O substitution by F seems promising approach to improve the cathode performance. Some of the prominent cathode materials doped with various metal cation at different lattice sites are given in the Table 1.

Table 1. Effect of dopant, doping site and optimum dopant value on performance of Perovskite/Double perovskite.

Perovskites/Double Perovskites	Doping	Opt. value of dopant (%)	Doping Site	Cell- configuration Electrolyte/ Anode (Cell type)	Test-ing temp. (°C)	Rp (Ω.cm²)	Power density mW.cm⁻² (of cathode material)	TEC (10^{-6} K^{-1})	Cell Test-ing Time (hr)	Ref.
$Nd_{1-x}Ln_xBaCo_2O_6$	Ln = La, Sm & Gd	La = 0.1	A - site	YSZ/ (CGO Buffer layer)/NiO-$Zr_{0.85}Y_{0.15}O_{1.95}$(Single cell)	700	0.083	1.045 W.cm⁻²	-	100 hrs	[20]
$Ba_{0.5}Sr_{0.5}Co_{0.2}Fe_{0.7}Mo_{0.1}O_{3-d}$	Mo	Mo = 0.1	B - site	YSZ/ $Ba_{0.5}Sr_{0.5}Co_{0.2}Fe_{0.7}Mo_{0.1}O_{3-d}$ (BSCFM) (Symmetrical cell)	800	0.035	418 (At 700 °C in H_2 with 3% water)	-	115 hrs	[22]

 doi:10.20944/preprints202405.0747.v1

$PrBaCo_{2-x}Mo_xO_{5+p}$	Mo (x = 0-0.07)	Mo = 0.03	B-site	SDC/NiO-SDC (Single Cell)	700	0.067	339	18.1	42 hrs	[23]
$PrBaCo_2O_{5+}F_x$ (O-site doping)	x = 0-0.2 %	F- = 0.1	O - site	GDC/Ni-GDC (Single cell)	650	0.062	0.679 W.cm^{-2}	17.46	100 hrs	[36]
$BaFeO_{3-\delta}$	La^{+3}, $Sm^{+3,}$ Gd^{+3} (A-Site) Zr^{+4} and Ce^{+4} (B-Site)	La^{+3} and Zr^{+4} = 0.005	A - site and B - site	SDC/$Ba_{0.9}La_{0.05}$ $FeO_{3-\delta}$ (BFO) (A-site Symmetrical cell) SDC/$BaFe_{0.95}Zr_{0.05}O_{3-\delta}$ (BFO) (B-site Symmetrical cell)	700	0.029 (La^{+3} at A-Site) 0.020 (Zr^{+4} B-Site)	-	-	-	[38]
$La_{0.6-x}M_xSr_{0.4}Co_{0.2}Fe_{0.8}O_3$	M = Ca, Ba & Bi	Bi = 0.2 %	A - site	YSZ/$La_{0.4}Bi_{0.2}Sr_{0.4}Co_{0.2}Fe_{0.8}O_3$(LBSCF (Symmetrical cell)	750	0.132	1.002 W.cm^{-2}	18.1	100 hrs at 600 °C	[15]
$Ln_xBa_{1-x}Co_{0.5}Fe_{0.3}O_{3-\delta}$ (Ln_xBCF)	Ln = La, Pr, Nd	Pr = 0.1 %	A - site	SDC/$Pr_{0.1}Ba_{0.9}Co_{0.5}Fe_{0.3}O_{3-\delta}$ (Symmetrical cell)	700	0.026 (ASR)	1236	16.2	150 hrs	[39]
$La_{2-x}A_xNi_{1-y}B_yO_{4+\delta}$ (LNO)	x = Pr y = Co	Pr =0.5 % Co = 0.2 %	A-site and B-site	YSZ/$La_{1.5}Pr_{0.5}Ni_{0.8}Co_{0.2}O_{4+\delta}$ (LPNCO) (Symmetrical cell)	600	1.95	400	-	-	[33]
$Pr_{2-x}La_xNi_{0.85}Cu_{0.1}Al_{0.05}O_{4+\delta}$	x = La	La = 1 %	A-site	LSGM/$PrLaNi_{0.85}Cu_{0.1}Al_{0.05}O_{4+\delta}$ (Symmetrical cell)	700	0.037 (ASR	341 (at 700 °C)	14.6	72 hrs	[34]

 doi:10.20944/preprints202405.0747.v1

						at 800 °C)				
$Ba_{0.5}Sr_{0.5}(Co_{0.8}Fe_{0.2})_{1-x}Zn_xO_{3-\delta}$ (BSCFZ)	x = Zn^{+2}	Zn^{+2} = 0.04 %	B - site	YSZ/$Ba_{0.5}Sr_{0.5}(Co_{0.8}Fe_{0.2})_{0.96}Zn_{0.04}O_{3-\delta}$ (BSCFZ) (Symmetrical cell)	600	0.23	0.58 W.cm^{-2}	-	140 hrs	[31]
$Ba_{0.5}Sr_{0.5}Co_{0.8-x}Fe_{0.2}Nb_xO_{3-\delta}$ (BSCFNb)	y = Nb	Nb = 0.05 %	B - site	SDC/NiO-$BaZr_{0.1}Ce_{0.7}Y_{0.2}O_{3-\delta}$ (Single cell)	700	1.14	882	18.74	70 hrs	[35]
$La_{1-x}Ce_xSr_{0.4}Co_{0.2}Fe_{0.8}O_3$ (LCSCF)	x = Ce^{+3}	Ce^{+3} = 0.6 %	A - site	GDC/Pt (Single cell)	750	0.09	-	-	-	[25]

3.2. Composites

To induce thermal compatibility between cathode and the electrolyte, the use of composite cathodes has been observed to be a promising approach. This also helps in formation of new oxygen ion transport channels throughout the electrodes and extend the TPB which can significantly enhance the oxygen reduction reaction.

The layered Perovskites like $SmBaSrCaCoFeO_{5+\delta}$ (SBSCCF) with the general formula of $AA'B_2O_{5+\delta}$ exhibits stacked layered structure that provides high oxygen diffusivity and O_2 transport coefficient. However, these materials suffer from high TEC due to the spin state of the transition metal. Wang et al. [40] studied the effect of addition of electrolyte material (GDC) up to 50% in cathode material $SmBa_{0.5}Sr_{0.25}Ca_{0.25}CoFeO_{5+\delta}$. They observed a decrease in TEC with increasing amount of GDC. Although the electrical conductivity of the composite material was less than the optimum value required for a good cathode material in SOFC operation (100 S.cm^{-1}) but this improved the power output by 75%. This is mainly expected to be due to the increase in TPB for the reaction.

Similarly, Ferrites have also been studied with various mixed ion conducting phases as composite cathodes. Gao et al. [41] used GDC in $Bi_{0.5}Sr_{0.5}FeO_{3-\delta}$-$Ce_{0.9}Gd_{0.1}O_{1.95}$ and reported a power density of 709 mW.cm^2 with 30 wt.% of GDC. It has been observed that optimum amount of ion conducting phase prevents the aggregation of the cathode particles and provide improved microstructure. Most of the researchers reported the use of ion conducting phase between 30-40 wt.% with different single/double perovskites. Doped ceria is commonly used in composites due to high ionic conductivities as shown in Figure 5.

Preprints.org (www.preprints.org) | NOT PEER-REVIEWED | Posted: 13 May 2024 doi:10.20944/preprints202405.0747.v1

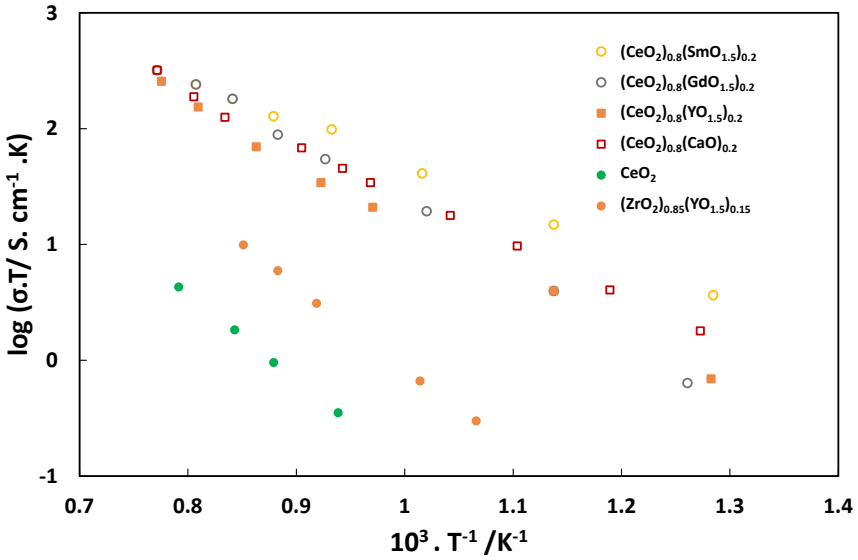

Figure 5. Arrhenius plots for ionic conductivities of ceria-based oxides. Figure redrawn from [42].

Although fluorites for electrochemical reactions as a composite have been extensively used for solid oxide fuel cell as well as electrolysis applications but there are very limited studies on their use as single withstanding electrode due to low electronic conductivity [43].

Similarly, the composite formation between other variety of combination/composition are also explored like LSM/SDC [44] and $PrBaCoO_{6-\delta}$/$PrBaCoTaO_6$ (PBC/PBCT) by Antipinskaya et al. [45] . In the latter study a composite cathode material PBC/PBCT having similar TEC demonstrated thermal compatibility with electrolyte (SDC), while maintaining low chemical interaction.

3.3. Infiltration/Impregnation

Infiltration technique has been reported to be effective for performance improvement of cathode materials. Conventionally, it consists of depositing thin films or nanoparticles of electrocatalytically active cathode materials into ion conducting framework such as YSZ, ScSZ, GDC etc. The most attractive feature is wide range of catalytic active materials can be used in combination with MIEC [46–48] as discussed below.

Effect of Infiltration on TPB

The oxygen ion conduction in pure ionic conductors is only along two-phase boundary (cathode and electrolyte surface) while in mixed ionic and electronic conductors, the ORR is extended to the whole cathode-electrolyte interface called TPB. A schematic representation of the oxide ion conduction in MIEC and pure ionic conductors is depicted in Figure 6. The extension of the triple phase boundary (TPB) is achieved by infiltrating ion conducting material [49]. The most frequently used MIEC are LSCF (Sr doped Lanthanum cobalt ferrite) [50], BSCF (Sr doped Barium Cobalt Ferrite), LSM (Sr -doped lanthanum manganite), LSC (Sr doped lanthanum cobaltite) [51] and LCN ($La_{0.95}Co_{0.4}Ni_{0.6}O_3$) [52] etc. Schematic representation of infiltration is depicted in Figure 7. Doped ceria is the material of interest because of high ionic conductivity and a good chemical and thermal compatibility with cobaltites [53]. Doped CeO_2 nanoparticles on the LSCF surface can improve the surface exchange co-efficient due to the introduction of additional oxygen vacancies. . Significant improvement of 59% and 50% in Rp is reported when infiltrated SDC in LSCF at 650 ℃ and at 750 ℃ as compared to parent cathode by Nie et al. [54] in LSCF-$Sm_{0.2}Ce_{0.8}O_{2-x}$.

Preprints.org (www.preprints.org) | NOT PEER-REVIEWED | Posted: 13 May 2024 doi:10.20944/preprints202405.0747.v1

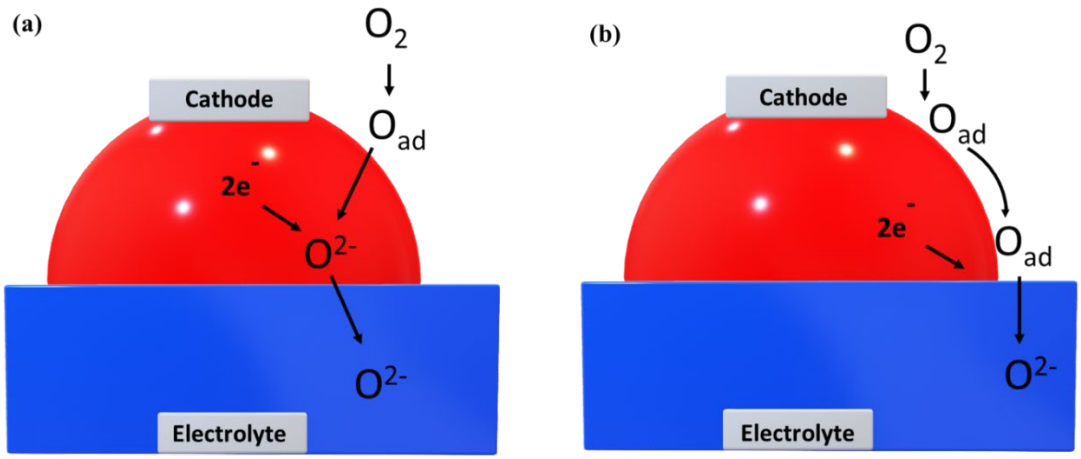

Figure 6. Oxygen conduction path (A) Triple phase Boundary (TPB) in MIEC cathodes (B) Two phase boundaries in non-MIEC cathodes. Figure redrawn from [55].

In addition, uniform distribution of the infiltrate can be achieved by controlling several extrinsic factors like the wetting property of the composite backbone by using organic solvents [56]. The epitaxy deposition of SSC nanoparticles on the LSCF-GDC composite cathode surface, can also result in a good contact between electrolyte and LSCF-GDC composite cathode interface as reported by Song et al. [57].

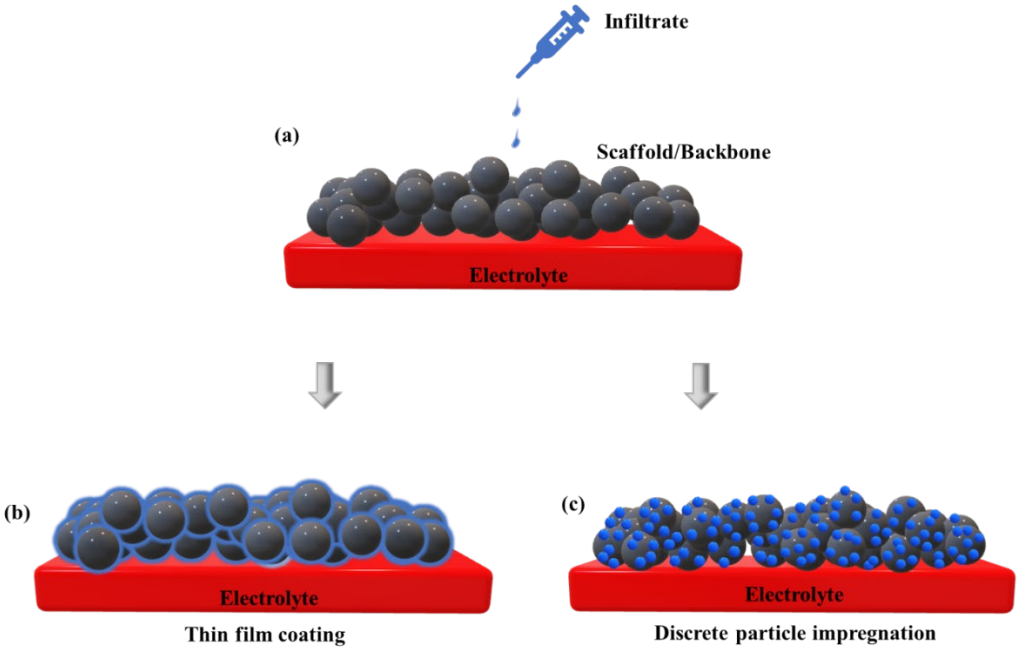

Figure 7. Two types of infiltration: a) Solution infiltration on backbone; b) Thin film coating; c) Discrete particle coating.

3.4. Core-Shell Composites

Core-Shell assembly is emerging as a new strategy to explore the new combination of materials. Several groups around the world are adopting new approaches to achieve the stable and efficient core shell cathode material. A variety of combination of the ion conducting phase as core while MIEC as the shell and vice versa have been investigated as shown in Table 2. Lee et al. [58] reported controlling the particle size of the SDC (50 nm) /LSCF core/shell material resulting in well distributed MIEC phase shell (LSCF) to cover evenly the surface of the core underneath. This helps in increasing

 doi:10.20944/preprints202405.0747.v1

the electrocatalytic activity and durability of the system over multiple thermal cycles. Ai et al. [59] used the rapid sintering treatment with thermal cycle of 20 secs to deposit the LSCF Shell on to the LSM core to take advantage of the electrocatalytic activity of the LSCF and durability of the LSM core with electrolyte while controlling coarsening of particles.

Table 2. Rp and power density of some of the core-shell cathodes.

Core shell Cathode	Electrolyte	Temperature (°C)	Rp ($\Omega.cm^2$)	Power density ($W.cm^{-2}$)	Reference
Ag@SDC	SDC	450	0.7	0.0562	[60]
Au@Ni	GDC	500	0.25	0.464	[61]
$YCo_{0.5}Fe_{0.5}O_3$(YCF)@$Gd_{0.1}Ce_{0.9}O_{1.95}$(GDC)	GDC	550	0.66	0.4265	[62]
Ag @ $Pr_{0.2}Ce_{0.8}O_{2-\delta}$ -LSCF	SDC	550	0.65	-	[63]
$La_{0.8}Sr_{0.2}MnO_{3-\delta}$ (LSM)@$Ba_{0.5}Sr_{0.5}Co_{0.8}Fe_{0.2}O_{3-\delta}$(BSCF)	GDC	600	1.141	-	[64]
$Sm_{0.5}Sr_{0.5}CoO_3$ (SSC)@$Sm_{0.2}Ce_{0.8}O_{1.9}$	SDC	650	0.098	1.07 (600 °C)	[65]
$La_{0.6}Sr_{0.4}Co_{0.2}Fe_{0.8}O_{3-\delta}$(LSCF)@$La_{0.6}Sr_{1.4}Co_{0.2}Fe_{0.8}O_{4-\delta}$ (LSCF)	SDC	650	0.17	0.57	[66]
$La_{0.8}Sr_{0.2}MnO_3$ (LSM)@$La_{0.6}Sr_{0.4}Co_{0.2}Fe_{0.8}O_{3-\delta}$ (LSCF)	YSZ	700	2.1	-	[59]
$PrBa_{0.5}Sr_{0.5}Co_{1.5}Fe_{0.5}O_{5+\delta}$ (PBSCF)-$La_2NiO_{4+\delta}$ (LN)	YSZ	700	0.51	0.71	[67]

 doi:10.20944/preprints202405.0747.v1

$LaCoO_{3-d}$ (LC)@$Ba_{0.5}Sr_{0.5}Co_{0.8}Fe_{0.2}O_{3-\delta}$ (BSCF)	GDC	750	0.020	0.929	[68]
$La_{0.8}Sr_{0.2}Co_{0.2}Fe_{0.8}O_{3-\delta}$ (LSCF)@$Gd_{0.2}Ce_{0.8}O_{1.9}$ (GDC)	GDC	750	0.16	-	[69]
$LaSrCoO_{4\pm\delta}$(LSC) @$La_{0.5}Sr_{0.5}CoO_{3-\delta}$ (LSC)	LSGM	800	0.03	0.87	[70]

Using nanofibrous forms of the cathode materials with casual arrangement of MIEC and ionic phases in Core-shell assembly also helps in modification of the microstructure and avoid aggregation upon sintering [62]. Nanofibrous microstructures are proven durable during operation due to uninterrupted oxygen diffusion and increment in TPB [71]. An efficient cathode with hollow nanofiber morphology resulting in increased ORR, and thus high power density of 1.11 $W.cm^{-2}$ at 550 ℃ has been reported to be due to virtuous oxygen diffusion [72]. Similarly, Zhang et al. [73] reported 5 times improvement in cathode polarization resistance of LSCF/CeO_2 nanofiber composite as compared to bare LSCF cathode.

3.5. Interface /Interfacial Layer Modifications

There are additional intrinsic and extrinsic factors that can lead to degradation of the cathode performance like interfacial diffusion of the metal cation into electrolyte resulting in insulating phase layer formation at the reaction interfaces. Multiple reports on interfacial cross reaction between cathode and electrolytes (GDC, SDC and even YSZ) at high temperatures suggest the need of interfacial modifications.

Sr segregation on the LSCF/YSZ phase is reported by Horita et al.[74]. The formation of the Sr segregation at LSCF/GDC/YSZ was evident from the SIMS (secondary ion mass spectrometry) analysis, by the high peak intensity of the ^{18}O at the GDC/YSZ interface. The Sr segregation was also evident from the SEM images which showed the $SrZrO_3$ layer near GDC/YSZ interface and the results were supported by EDS mapping. They explained two possible reasons for $SrZrO_3$ formation for the high ^{18}O peak intensity (i) the voltage assisted faster incorporation of ^{18}O near GDC/YSZ at the increased polarization (ii) other possibility is the hindrance of ^{18}O diffusion across the Sr segregation layer due to lower ion diffusivity which caused the delay in transport of the ^{18}O from GDC/YSZ area.

Two types of interdiffusion of elements in LSCF/GDC cathode electrolyte interface are reported by Li et al. [75]. First is the mutual diffusion of elements between cathode and electrolyte. The STEM-EDX analysis was performed which showed that the interdiffusion of the cation Sr or La, Co as well as Fe from LSCF cathode into the electrolyte can take place across interface. From the comparison of the ionic radii of the cations and their diffusion length or distance from interface, the mutual interdiffusion was suggested as preferable diffusion mechanism. This mutual diffusion can extend up to 200 nm in diameter from interface.

The second type of diffusion is around the grain boundaries as it is believed that grain boundaries give the pathways for the segregation of the cations. The presence of the La and other A-site cations near grain boundary having similarity between ionic radii of the elements on the two sides made them diffuse around grain boundaries.

 doi:10.20944/preprints202405.0747.v1

The other factor that dictates the resistance at the interface between cathode and electrolyte is the effect of sintering temperature on the microstructure. The higher sintering temperature results in the grain agglomeration leading to coarsening of the particles while lower sintering temperature cause the incomplete or poor connection, both the scenario contributes to the increased resistance of cathode/interlayer.

Jang et al. [76] thoroughly investigated the performance efficiency of the bilayer system LSCF/GDC/YSZ interface as a function of sintering temperature. They reported the increased performance of the nanoweb structured LSCF cathode deposited on the electrolyte with GDC barrier layer. Impurities segregation takes place towards the cathode/electrolyte interface above the optimum sintering temperature range (1250℃), while splitting/ruptures in the deposited GDC layer sintered is reported when at lower temperatures. In this comprehensive study of effect sintering temperature on morphology of the cathode material, the main area of concern was the GDC/YSZ interfacial layer where the Ce-Zr layer deposition caused the increased polarization resistance. But, further work is required regarding the changes to TPB and explanation of the oxygen ion transport.

The interlayer can prevent the formation of the resistive phases for achieving high power density. Park et al. [77] applied the interlayer of GDC at the LSCF/GDC interface. By optimizing the heat treatment during calcination, they were able to suppress the formation of the secondary insulating phases with Sr or Zr. However, thickness of the interlayer can increase the ionic transport resistance and therefore increase in the overall resistance of the cell.

Importantly, substantial modification to the interface can be done by depositing catalyst interfacial layer between cathode and electrolyte. The infiltrated catalyst interfacial layer must meet certain performance criteria for example, it should be chemically stable and have a thermal expansion compatibility between cathode and electrolyte.

4. Modifications to Cathode to Mitigate Carbon Dioxide (CO_2) and Humidity Effect

The presence of CO_2 and humidity in reactant gas (Air, oxygen) can significantly affect the performance of the cells. For example, CO_2 adsorption competes with O_2 adsorption on the active sites of the cathode and thus hindering ORR at the cathode. Notably , mechanism of the CO_2 adsorption depends upon the nature of the cathode material and configuration for example, the effect of the CO_2 exposure on the ORR in pure electronic conducting materials like LSM (where ORR is confined to the TPB) is different from the MIEC cathode material (where ORR takes place over the entire cathode rather than only at TPB).

Another important factor effecting the response of the cathode material towards CO_2 exposure is the working temperature of the cell. The temperature dependent response towards the CO_2 exposure in pure electronic conducting cathode material and in MIEC cathode materials is different due to the difference in the chemical composition, microstructure as well as the catalytic nature [78]. Enhanced CO_2 tolerance of different cathode materials is studied by exploring various strategies. Almar et al. [79] reported that using acidic 10% Y^{+3} doping showed an improvement not only in ORR but also the resistivity of BSCF in CO_2 atmosphere which according to Lewis acid base theory is less likely to be affected by acidic nature of CO_2.

The improved bond energy of metal-oxygen by substitution of Cobalt with certain metals, stabilizes the chemical structure thus decreasing the chemical adsorption of CO_2. Alkaline earth metal (Sr, Ba) containing cathode materials have been reported to form carbonates in CO_2 containing environment that rapidly degrades the cathode material for ORR Hu et al. [80] reported improvement and stability of antimony (Sb) doped strontium cobalt oxide ($SrCoO_{3-\delta}$) in 10% CO_2/air atmosphere due to increased metal to oxygen bond energy. Doping 18.75% Sb shows lower affinity to carbonates as compared to lower content of Sb doping in $SrCoO_{3-\delta}$.

Similarly, cell operating in humid air can affect the cathode performance. Like CO_2, it is believed that water vapours undergo a competitive adsorption for active sites and thus hinder ORR. Huang et al. [81] reported severe oxygen partial pressure dependent effect of humidity, on HT-SOFC LSM cathode material as compared to IT- SOFC cathode material - LSC [81] with more hostile effect at lower temperature than high temperature [82]. This is evident from Figure 8 showing the more

 doi:10.20944/preprints202405.0747.v1

pronounced effect of humidity and even CO_2 on stability of LSCF cathode material at lower temperature 600 °C as compared to 750 °C under same operating conditions [82]. This suggests the interaction of these cathode material with humidity is dictated by the material chemistry along with external factors.

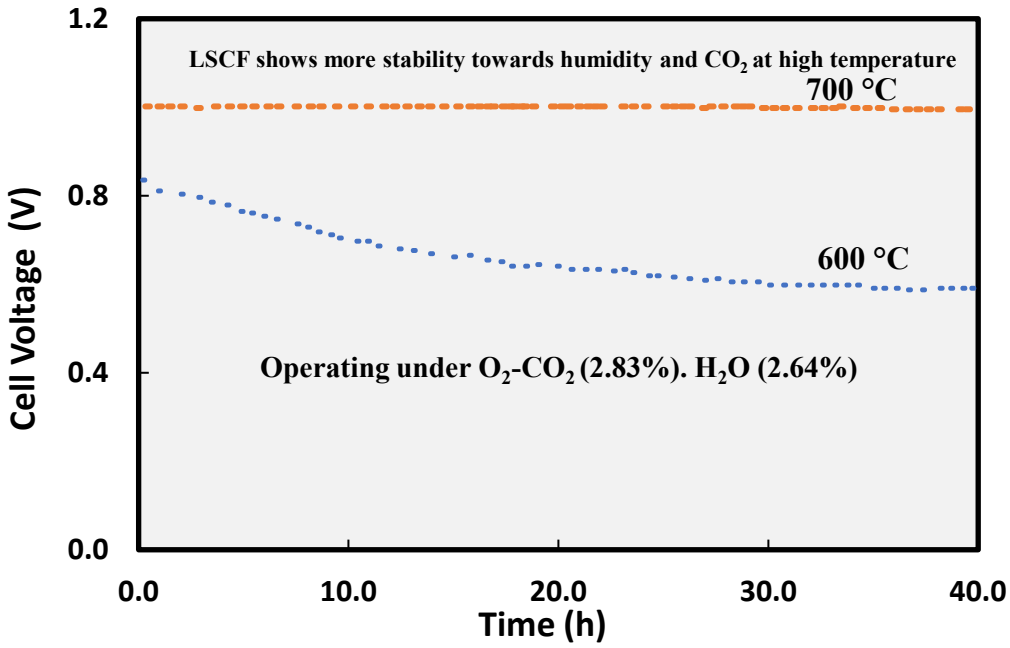

Figure 8. LSCF Stability behaviour at low (600 ℃) and high (700 ℃) temperature in CO_2 and humidity exposure test. Figure redrawn from [82].

LSCF:GDC composite showing more tolerance to humidity has been reported in the literature even at high vapour content as compared to LSM:YSZ [83]. LSM:YSZ composite showed reversible performance in dry air. Interestingly OCV was considerably stable suggesting that humidity response under voltage is totally reflected by polarization resistance. The possible explanation of the LSM:YSZ composite ORR degradation is the Sr segregation and surface morphology change. [84]. U.S department of energy reported in a project some of the fundamental concepts for difference in mechanism of Sr segregation between LSM:YSZ and LSCF:GDC. They stated the Sr segregation is directly dependent on Sr-content along with Mn and La segregation that is also reported at interface towards YSZ. According to Chen et al. [85] ORR at TPB is also affected by humidity due to MnO_x insulating phase formation which engorged towards the interface over time (Figure 9).

 doi:10.20944/preprints202405.0747.v1

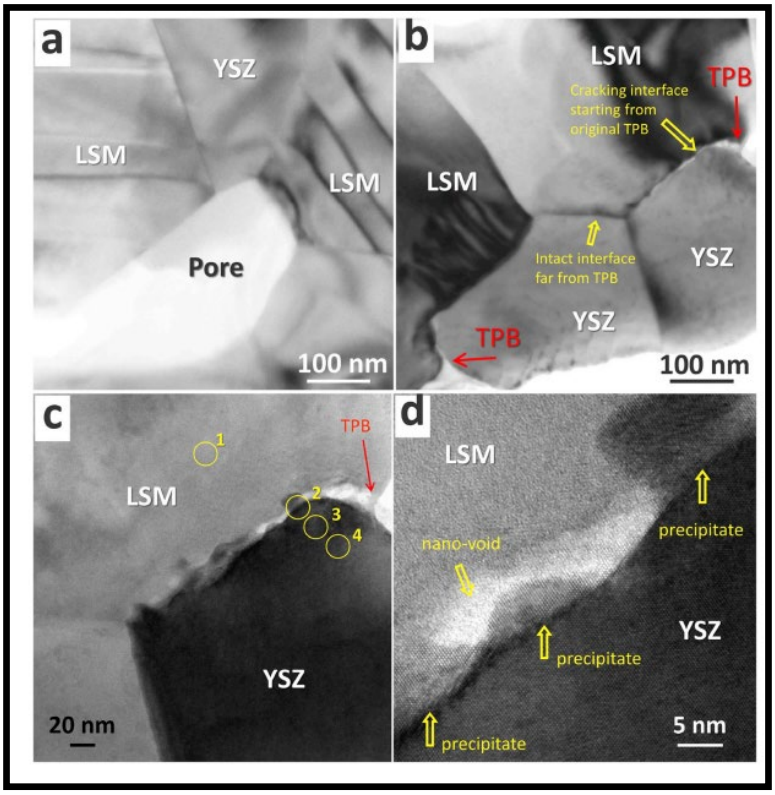

Figure 9. a) TEM image of the original TPB region and the LSM/YSZ interface in the fresh cell. b) TEM image of the active layer of cell operated for 120 h. The interfacial defects initiate from the original TPBs, while the LSM/YSZ interface and YSZ/YSZ grain boundaries initially remain intact. c) An enlarged TPB region in b showing the cracking at the LSM/YSZ interface is associated with the nano precipitates. d) An enlarged TPB region in b showing the precipitates have an epitaxial orientation with the YSZ grains and showing an amorphous layer at the LSM/YSZ interface. Figure used from [85] with permission.

In case of LSCF, H_2O molecules chemically bound to Co, thus filling the lattice vacancies, and hindering oxygen transport. Co (cobalt) and Fe (Iron) percentage content are seemed to be interfering with degree of lattice expansion/contraction with higher percentage iron containing LSCF lattice showing more expansion with humidity [86].

Similarly, a comparative study of electrochemical performance and Cr poisoning in humid conditions between LSM:YSZ and LSF:GDC composite was carried out by Wang et al. [87]. The results suggested that LSF:GDC composite is less affected in humid air comparatively, and even showed improved electrochemical performance because of the presence of H_2O molecules in ambient environment. Nanocrystals of Sr accumulation on the surface in presence of humid air was reported in LSC ($La_{6.0}Sr_{4.0}CoO_{3-\delta}$) by Egger et al. [88] who studied the dominant effect of microstructure and synthesis method in offering the protection against humidity to LSC material. The LSC infiltrated on GDC scaffolds with larger surface area and optimum pore content in microstructure was reported helpful in providing stability in humid air. Thus, approaches like doping with metals which are believed to increase the stability of the cathode material are tested for increasing the stability in humid conditions [89]. Good adhesion between cathode and electrolyte is also reported to decrease the humidity adverse effect on cathode than unimproved interface [90]. The composite formation in core shell assembly by introducing protective layer is reported to have improved humidity tolerance of different cathode material for IT-SOFC.

 doi:10.20944/preprints202405.0747.v1

5. Conclusion

Perovskites are the material of choice for cathode at intermediate temperature SOFC operation. The unique electrical characteristics offered by the two metals in the crystal lattice, provide a substantial scope for R&D towards optimisation of the cathode properties. The possibility of vast variety of dopants at A- site and/or B-site can offer improved electrical conductivity due to mixed valence cation formation (M^{+3}/M^{+4} or M^{+2}/M^{+3}). Dopants such as rare earth metals, alkaline earth metals and transition metals of stable oxidation states and similar ionic radius have been explored as a substitution in perovskites particularly, iron containing perovskites. In addition to improvement in electronic conductivity, secondary phase formation and stability can also be tailored by such substitutions. Interestingly, non-metallic substitution at O-site has also been demonstrated and shown improved electrical conductivity and TEC simultaneously. However, this strategy has not been widely explored.

The cathode characteristics improved by doping does not meet all the requirements for a good cathode material in terms of the thermal compatibility with electrolyte and conductivities. On the other hand, composite formation between the cathode material such as cobaltites, manganite or ceria-based cathode materials and the electrolyte material (doped ceria or doped zirconia) results in improvement in TEC compatibility as well as in the extension of TPB. However, co-sintering of the constituent phases often results in the insulating phase formation or agglomeration along the grain boundary in the extended active area (TPB) resulting in the degradation of the performance. Optimization of sintering temperature, doping levels could help in the improved performance while controlling the growth of secondary phases.

Non-uniform infiltration can also disrupt the oxygen conduction path which can significantly affect the performance of SOFC. The interfacial modification by smearing barrier layers of micro/nm range through different advanced techniques can control the cross diffusion across the interfaces. This review suggests that role of ionic barrier layers on ORR mechanism and kinetics is still not clear suggesting the direction of the future research in this field.

Acknowledgment: This review was supported by the CSIRO Hydrogen Future Science Platform (FSP). The authors would also like to acknowledge Royal Melbourne Institute of Technology (RMIT), Melbourne, Australia for Collaborating in this review. We are thankful to Dr. Dattatray Dhawale for reviewing of the manuscript.

Abbreviation

SOFC	Solid Oxide Fuel Cell
HT-SOFC	High-Temperature solid oxide fuel cell
IT-SOFC	Intermediate Temperature solid oxide fuel cell
SOEC	Solid oxide electrolysis cell
PEMFC	Polymer electrolyte membrane fuel cell
ORR	Oxygen reduction reaction
TPB	Triple phase boundary
NOx	Oxides of nitrogen
SOx	Oxides of Sulphur
DES	Distributed Energy system
BOP	Balance of plant
NG	Natural gas
OCV	Open circuit voltage
ABO_3	A general formula for Perovskites
MIEC	Mixed ionic and electronic conductor

 doi:10.20944/preprints202405.0747.v1

Ni-YSZ	Nickle-Yttrium stabilized zirconia
YSZ	Yttrium stabilized zirconia
ScSZ	Scandium stabilized zirconia
GDC	Gadolinium doped ceria
SDC	Samarium doped ceria
LSGM	Strontium magnesium doped Lanthanum gallate
LSM	Lanthanum strontium manganite
LSCF	Lanthanum (La) Strontium (Sr) Cobalt (Co) ferrite
BSCF	Barium (Ba) Strontium (Sr) Cobalt (Co) ferrite
SSC	Samarium (Sm) doped Strontium (Sr) cobalt oxide
R&D	Research and development
ASR	Area-specific resistance
TGA	Thermal Gravitational Analysis
SEM	Scanning Electron Microscope
SIMS	Secondary Ion Mass Spectroscopy
EDS	Energy Dispersive Spectroscopy

Symbols

δ	Oxygen non-stoichiometry
K^{-1}	Per Kelvin
$S.cm^{-1}$	Siemens per centimetre
V_f	Free oxygen volume
D*	Electronic conductivity
R_p	Cathode Polarization/resistance
R_{ohm}	Electrolyte polarization/resistance
E_a	Activation energy
R	Ionic radius
a,b,c	Lattice parameters of the cubic system along with three the dimensions
$\Omega.cm^2$	Ohms centimetre square
$W.cm^{-2}$	Watt per centimetre square
$mW.cm^{-2}$	Milliwatt per centimetre square
Ln	Rare earth metals

References

1. *Australia's Department of Industry, Innovation, and Science, Office of the Chief Economist, Australian Energy Update 2021, pg 27-30.*
2. Chen, J. and M. Ni, *Economic analysis of a solid oxide fuel cell cogeneration/trigeneration system for hotels in Hong Kong.* Energy and Buildings, 2014. 75: p. 160-169.

 doi:10.20944/preprints202405.0747.v1

3. Baldi, F., et al., *A Cogeneration System Based on Solid Oxide and Proton Exchange Membrane Fuel Cells With Hybrid Storage for Off-Grid Applications.* 2019. 6.
4. Song, B., et al., *Quantification of the degradation of Ni-YSZ anodes upon redox cycling.* Journal of Power Sources, 2018. 374: p. 61-68.
5. Jiao, Z., et al., *Quantitative Study on the Correlation Between Solid Oxide Fuel Cell Ni-YSZ Composite Anode Performance and Sintering Temperature Based on Three-dimensional Reconstruction.* Journal of the Electrochemical Society, 2012. 159(7): p. F278-F286.
6. Iwata, T., *Characterization of Ni-YSZ anode degradation for substrate-type solid oxide fuel cells.* Journal of the Electrochemical Society, 1996. 143(5): p. 1521-1525.
7. Liu, Y., et al., *Development of nickel based cermet anode materials in solid oxide fuel cells – Now and future.* Materials Reports: Energy, 2021. 1(1).
8. Vafaeenezhad, S., et al., *Microstructure and long-term stability of Ni–YSZ anode supported fuel cells: a review.* Materials Futures, 2022. 1(4): p. 042101.
9. Heidarpour, A., et al., In situ *fabrication mechanism of a dense Sr and Ca doped lanthanum chromite interconnect on Ni-YSZ anode of a solid oxide fuel cell during co-sintering.* Ceramics international, 2013. 39(2): p. 1821-1826.
10. Horita, T., *Microstructures and oxygen diffusion at the LaMnO3 film/yttria-stabilized zirconia interface.* Solid state ionics, 2002. 152-153: p. 439-446.
11. Hussain, S. and L.J.E.T. Yangping, *Review of solid oxide fuel cell materials: cathode, anode, and electrolyte.* 2020: p. 1-14.
12. Zhang, L., et al., *Improved thermal expansion and electrochemical performances of Ba0.6Sr0.4Co0.9Nb0.1O3−δ–Gd0.1Ce0.9O1.95 composite cathodes for IT-SOFCs.* International journal of hydrogen energy, 2014. 39(15): p. 7972-7979.
13. Yin, S., et al., *Study of Sm0.2Ce0.8O1.9 (SDC) electrolyte prepared by a simple modified solid-state method.* Journal of Rare Earths, 2014. 32(8): p. 767-771.
14. Fan, B., J. Yan, and X. Yan, *The ionic conductivity, thermal expansion behavior, and chemical compatibility of La0.54Sr0.44Co0.2Fe0.8O3-δ as SOFC cathode material.* Solid State Sciences, 2011. 13(10): p. 1835-1839.
15. Jia, W., et al., *Flexible A-site doping La0.6-xMxSr0.4Co0.2Fe0.8O3 (M=Ca, Ba, Bi; x=0, 0.1, 0.2) as novel cathode material for intermediate-temperature solid oxide fuel cells: A first-principles study and experimental exploration.* Journal of Power Sources, 2021. 490.
16. Jung, W. and H.L. Tuller, *Investigation of surface Sr segregation in model thin film solid oxide fuel cell perovskite electrodes.* Energy & Environmental Science, 2012. 5(1): p. 5370-5378.
17. Liu, Q., et al., *Perovskite Sr2Fe1.5Mo0.5O6−δ as electrode materials for symmetrical solid oxide electrolysis cells.* International Journal of Hydrogen Energy, 2010. 35(19): p. 10039-10044.
18. Dey, S., et al., *Synthesis and characterization of Nanocrystalline Ba0·6Sr0·4Co0·8Fe0·2O3 for application as an efficient anode in solid oxide electrolyser cell.* International Journal of Hydrogen Energy, 2020. 45(7): p. 3995-4007.
19. Stevenson, J.W., et al., *Electrochemical Properties of Mixed Conducting Perovskites La1 − x M x Co1 − y Fe y O 3 − δ (M = Sr, Ba, Ca).* Journal of The Electrochemical Society, 1996. 143(9): p. 2722-2729.
20. Anbo, Y., et al., *Effects of rare earth doping on electrochemical properties of NdBaCo2O6- cathode materials.* Journal of Alloys and Compounds, 2020. 837.
21. Barros Julião, P.S., *A-site cation influences on performance, structure and conductivity of a lanthanide-based perovskite electrode for symmetrical solid oxide fuel cells.* Journal of Power Sources, 2020. 450.
22. Yang, X., et al., *Improving stability and electrochemical performance of Ba0.5Sr0.5Co0.2Fe0.8O3-δ electrode for symmetrical solid oxide fuel cells by Mo doping.* Journal of Alloys and Compounds, 2020. 831.
23. Xu, J., et al., *Characterization of high–valence Mo–doped PrBaCo2O5+ cathodes for IT–SOFCs.* Journal of Alloys and Compounds, 2020. 842.
24. Sowjanya, C., et al., *Effect of B-site substitution on the crystal structure, electrical conductivity and oxygen transport properties of La0.5Sr0.5M0.2Fe0.8O3-δ (M = Co, Al, and Zn) perovskite.* Journal of Solid State Chemistry, 2020. 285.

 doi:10.20944/preprints202405.0747.v1

25. Zhou, F., et al., *Effects of cerium doping on the performance of LSCF cathodes for intermediate temperature solid oxide fuel cells.* International Journal of Hydrogen Energy, 2018. 43(41): p. 18946-18954.
26. Chen, K., et al., *Nb and Pd co-doped La0.57Sr0.38Co0.19Fe0.665Nb0.095Pd0.05O3-δ as a stable, high performance electrode for barrier-layer-free Y2O3-ZrO2 electrolyte of solid oxide fuel cells.* Journal of Power Sources, 2018. 378: p. 433-442.
27. Serra, J.M. and H.-P. Buchkremer, *On the nanostructuring and catalytic promotion of intermediate temperature solid oxide fuel cell (IT-SOFC) cathodes.* Journal of Power Sources, 2007. 172(2): p. 768-774.
28. Liu, Y., et al., *Enhanced electrochemical activity and stability of LSCF cathodes by Mo doping for intermediate temperature solid oxide fuel cells.* Journal of Applied Electrochemistry, 2021. 51(3): p. 425-433.
29. Zhu, Y., et al., *A permeation model study of oxygen transport kinetics of BaxSr1-xCo0.8Fe0.2O3-δ.* AlChE journal, 2020. 66(9).
30. Weber, V., et al., *Influence of B-site doping with Ti and Nb on microstructure and phase constitution of (Ba0.5Sr0.5)(Co0.8Fe0.2)O3−δ.* Journal of Materials Science, 2019. 55(3): p. 947-966.
31. Zeng, Q., et al., *A Zn-Doped Ba0.5Sr0.5Co0.8Fe0.2O3-δ Perovskite Cathode with Enhanced ORR Catalytic Activity for SOFCs.* Catalysts, 2020. 10(2).
32. Mushtaq, N., et al., *Perovskite SrFe1-xTixO3-δ (x <= 0.1) cathode for low temperature solid oxide fuel cell.* Ceramics International, 2018. 44(9): p. 10266-10272.
33. Navarrete, L., et al., *Tailoring La2-XAXNi1-YBYO4+δcathode performance by simultaneous A and B doping for IT-SOFC.* International Journal of Hydrogen Energy, 2020. 45(31): p. 15589-15599.
34. Zhou, Q., et al., *Preparation and electrochemical properties of an La-doped Pr2Ni0.85Cu0.1Al0.05O4+δcathode material for an IT-SOFC.* Journal of Alloys and Compounds, 2020. 824.
35. Huang, Y., et al., *Ba0.5Sr0.5Co0.8-xFe0.2NbxO3-δ (x≤0.1) as cathode materials for intermediate temperature solid oxide fuel cells with an electron-blocking interlayer.* Ceramics International, 2020. 46(8): p. 10215-10223.
36. Wan, Y., et al., *Thermal cycling durability improved by doping fluorine to PrBaCo2O5+δ as oxygen reduction reaction electrocatalyst in intermediate-temperature solid oxide fuel cells.* Journal of Power Sources, 2018. 402: p. 363-372.
37. Wang, W., et al., *Highly promoted performance of triple-conducting cathode for YSZ-based SOFC* via *fluorine anion doping.* Ceramics International, 2020.
38. Wang, J., et al., *The effect of A-site and B-site substitution on BaFeO3−δ: An investigation as a cathode material for intermediate-temperature solid oxide fuel cells.* Journal of Power Sources, 2015. 297: p. 511-518.
39. Zhang, W., et al., *Effective promotion of oxygen reduction activity by rare earth doping in simple perovskite cathodes for intermediate-temperature solid oxide fuel cells.* Journal of Power Sources, 2020. 446.
40. Wang, S., et al., *Effect of electrolyte composite on the performance of SmBa0.5Sr0.25Ca0.25CoFeO5+δ cathode for IT-SOFCs.* Ionics, 2019. 26(1): p. 281-291.
41. Gao, J., et al., *Improved electrochemical activity of Bi0.5Sr0.5FeO3-δ–Ce0.9Gd0.1O1.95composite cathode electrocatalyst for solid oxide fuel cells.* Ceramics International, 2021. 47(1): p. 748-754.
42. Eguchi, K., et al., *Electrical properties of ceria-based oxides and their application to solid oxide fuel cells.* Solid state ionics, 1992. 52(1): p. 165-172.
43. Ishihara, T., et al., *Bi doped Pr6O11 as fluorite oxide cathode for all-fluorite solid oxide fuel cells.* Journal of Power Sources, 2015. 275: p. 167-174.
44. Eksioglu, A., et al., *Formation of Nanocomposite Solid Oxide Fuel Cell Cathodes by Preferential Clustering of Cations from a Single Polymeric Precursor.* ACS applied materials & interfaces, 2019. 11(51): p. 47904-47916.
45. Antipinskaya, E.A., et al., *Electrochemical performance and superior CO2 endurance of PrBaCo2O6–δ–PrBaCoTaO6 composite cathode for IT-SOFCs.* Electrochimica Acta, 2021. 365: p. 137372.
46. Ding, X.F., et al., *Enhanced oxygen reduction activity on surface-decorated perovskite La0.6Ni0.4FeO3 cathode for solid oxide fuel cells.* ELECTROCHIMICA ACTA, 2015. 163: p. 204-212.

 doi:10.20944/preprints202405.0747.v1

47. Shen, J., et al., *Impregnated LaCo0.3Fe0.67Pd0.03O3-delta as a promising electrocatalyst for "symmetrical" intermediate-temperature solid oxide fuel cells.* JOURNAL OF POWER SOURCES, 2016. 306: p. 92-99.
48. Giuliano, A., et al., *Infiltration, Overpotential and Ageing Effects on Cathodes for Solid Oxide Fuel Cells: La0.6Sr0.4Co0.2Fe0.8O3-delta versus Ba0.5Sr0.5Co0.8Fe0.2O3-delta.* JOURNAL OF THE ELECTROCHEMICAL SOCIETY, 2017. 164(10): p. F3114-F3122.
49. Endler-Schuck, C., et al., *The chemical oxygen surface exchange and bulk diffusion coefficient determined by impedance spectroscopy of porous La0.58Sr0.4Co0.2Fe0.8O3−δ (LSCF) cathodes.* Solid state ionics, 2015. 269: p. 67-79.
50. Shah, M., P.W. Voorhees, and S.A. Barnett, *Time-dependent performance changes in LSCF-infiltrated SOFC cathodes: The role of nano-particle coarsening.* Solid State Ionics, 2011. 187(1): p. 64-67.
51. Song, X., et al., *Electrochemically influenced cation inter-diffusion and Co3O4 formation on La0.6Sr0.4CoO3 infiltrated into SOFC cathodes.* Solid State Ionics, 2015. 278: p. 91-97.
52. Ovtar, S., et al., *In-situ formed Ce0.8Gd0.2O1.9 barrier layers on yttria stabilized zirconia backbones by infiltration - A promising path to high performing oxygen electrodes of solid oxide cells.* Solid state ionics, 2017. 304: p. 51-59.
53. Hu, B., Y. Wang, and C. Xia, *Effects of Ceria Conductivity on the Oxygen Incorporation at the LSCF-SDC-Gas Three-Phase Boundary.* Journal of the Electrochemical Society, 2015. 162(1): p. F33-F39.
54. Nie, L., et al., *La0.6Sr0.4Co0.2Fe0.8O3−δ cathodes infiltrated with samarium-doped cerium oxide for solid oxide fuel cells.* Journal of Power Sources, 2010. 195(15): p. 4704-4708.
55. Muneeb Irshad, K.S., Rizwan Raza , et al., *A Brief Description of High Temperature Solid Oxide Fuel Cell's Operation, Materials, Design, Fabrication Technologies and Performance*. Vol. 6. 2016, ; : Appl. Sci.
56. Tomov, R.I., et al., *Performance optimization of LSCF/Gd:CeO2 composite cathodes* via *single-step inkjet printing infiltration.* Journal of Applied Electrochemistry, 2017. 47(5): p. 641-651.
57. Song, Y.-H., et al., *Facile surface modification of LSCF/GDC cathodes by epitaxial deposition of Sm0.5Sr0.5CoO3via ultrasonic spray infiltration.* Journal of materials chemistry. A, Materials for energy and sustainability, 2020. 8(7): p. 3967-3977.
58. Lee, S., et al., *Investigation of electrospun Ba0.5Sr0.5Co0.8Fe0.2O3−δ-Gd0.1Ce0.9O1.95 cathodes for enhanced interfacial adhesion.* International Journal of Hydrogen Energy, 2018. 43(46): p. 21535-21546.
59. Ai, N., K. Chen, and S.P. Jiang, *A La0.8Sr0.2MnO3/La0.6Sr0.4Co0.2Fe0.8O3−δ core–shell structured cathode by a rapid sintering process for solid oxide fuel cells.* International Journal of Hydrogen Energy, 2017. 42(10): p. 7246-7251.
60. Kamlungsua, K., et al., *Inkjet-printed Ag@SDC core-shell nanoparticles as a high-performance cathode for low-temperature solid oxide fuel cells.* International Journal of Hydrogen Energy, 2021. 46(60): p. 30853-30860.
61. Yang, T., et al., *The annealing influence on the microstructure and performance of Au@Ni core-shell bimetal as the cathode of low-temperature solid oxide fuel cells.* International Journal of Hydrogen Energy, 2015. 40(14): p. 4980-4988.
62. Yang, J., et al., *Electrospun Core–Shell Fibers for High-Efficient Composite Cathode-Based Solid Oxide Fuel Cells.* Energy & Fuels, 2021. 35(2): p. 1768-1778.
63. Ding, X., et al., *Enhancing oxygen reduction activity of perovskite cathode decorated with core@shell nano catalysts.* International Journal of Hydrogen Energy, 2019. 44(39): p. 22122-22128.
64. Qiu, P., et al., *Promoted CO2-poisoning resistance of La0.8Sr0.2MnO3−δ-coated Ba0.5Sr0.5Co0.8Fe0.2O3−δ cathode for intermediate temperature solid oxide fuel cells.* Journal of Power Sources, 2016. 327: p. 408-413.
65. Lee, D., et al., *Durable high-performance Sm0.5Sr0.5CoO3–Sm0.2Ce0.8O1.9 core-shell type composite cathodes for low temperature solid oxide fuel cells.* International Journal of Hydrogen Energy, 2011. 36(11): p. 6875-6881.
66. Wang, L., et al., *A novel core-shell LSCF perovskite structured electrocatalyst with local hetero-interface for solid oxide fuel cells.* International Journal of Hydrogen Energy, 2020. 45(20): p. 11824-11833.
67. Li, J., et al., *Microstructure optimization for high-performance PrBa0.5Sr0.5Co1.5Fe0.5O5+δ-La2NiO4+δ core-shell cathode of solid oxide fuel cells.* Journal of Power Sources, 2018. 379: p. 206-211.

68. Qiu, P., et al., *LaCoO3-δ coated Ba0.5Sr0.5Co0.8Fe0.2O3-δ cathode for intermediate temperature solid oxide fuel cells.* Electrochimica Acta, 2019. 319: p. 981-989.
69. Li, D., et al., *Study on durability of novel core-shell-structured La0.8Sr0.2Co0.2Fe0.8O3-δ@Gd0.2Ce0.8O1.9 composite materials for solid oxide fuel cell cathodes.* International Journal of Hydrogen Energy, 2021. 46(55): p. 28221-28231.
70. Li, F., et al., *LaSrCoO4±@La0.5Sr0.5CoO3- core-shell hybrid as the cathode materials for solid oxide fuel cells.* Journal of Alloys and Compounds, 2020. 819.
71. Kim, C., et al., *Ba0.5Sr0.5Co0.8Fe0.2O3-δ / Gd0.1Ce0.9O2-δ Core/shell Nanofiber* Via *One-Step Electrospinning for Cathode of LT-SOFCs*, in *ECS Trans*. 2017, The Electrochemical Society, Inc. p. 637-641.
72. Chen, Y., et al., *A durable, high-performance hollow-nanofiber cathode for intermediate-temperature fuel cells.* Nano energy, 2016. 26(C): p. 90-99.
73. Zhang, W., et al., *La0.6Sr0.4Co0.2Fe0.8O3−δ/CeO2 Heterostructured Composite Nanofibers as a Highly Active and Robust Cathode Catalyst for Solid Oxide Fuel Cells.* ACS Applied Materials & Interfaces, 2019. 11.
74. Horita, T., et al., *Visualization of oxide ionic diffusion at SOFC cathode/electrolyte interfaces by isotope labeling techniques.* Solid state ionics, 2014. 262: p. 398-402.
75. Li, Z.-P., et al., *Two types of diffusions at the cathode/electrolyte interface in IT-SOFCs.* Journal of solid state chemistry, 2011. 184(9): p. 2458-2461.
76. Jang, I., et al., *Interface engineering of yttrium stabilized zirconia/gadolinium doped ceria bi-layer electrolyte solid oxide fuel cell for boosting electrochemical performance.* Journal of power sources, 2019. 435: p. 226776.
77. Park, S.-Y., et al., *Ni–YSZ-supported tubular solid oxide fuel cells with GDC interlayer between YSZ electrolyte and LSCF cathode.* International journal of hydrogen energy, 2014. 39(24): p. 12894-12903.
78. Zhao, Z., et al., *A comparison on effects of CO2 on La0.8Sr0.2MnO3+δ and La0.6Sr0.4CoO3−δ cathodes.* Journal of Power Sources, 2013. 222: p. 542-553.
79. Almar, L., et al., *Improved Phase Stability and CO2 Poisoning Robustness of Y-Doped Ba0.5Sr0.5Co0.8Fe0.2O3−δ SOFC Cathodes at Intermediate Temperatures.* ACS Applied Energy Materials, 2018. 1(3): p. 1316-1327.
80. Hu, X., et al., *Antimony-doped strontium cobalt oxide as promising cathode for low-temperature solid oxide fuel cell with excellent carbon dioxide tolerance.* Applied Catalysis B: Environmental, 2021. 286.
81. Huang, Y.L., C. Pellegrinelli, and E.D. Wachsman, *Fundamental Impact of Humidity on SOFC Cathode ORR.* Journal of The Electrochemical Society, 2015. 163(3): p. F171-F182.
82. Zhao, Z., et al., *High- and low- temperature behaviors of La0.6Sr0.4Co0.2Fe0.8O3−δ cathode operating under CO2/H2O-containing atmosphere.* International Journal of Hydrogen Energy, 2013. 38(35): p. 15361-15370.
83. Nielsen, J., A. Hagen, and Y.L. Liu, *Effect of cathode gas humidification on performance and durability of Solid Oxide Fuel Cells.* Solid State Ionics, 2010. 181(11-12): p. 517-524.
84. Liu, R.R., et al., *Influence of water vapor on long-term performance and accelerated degradation of solid oxide fuel cell cathodes.* Journal of Power Sources, 2011. 196(17): p. 7090-7096.
85. Chen, Y., et al., *Interface and grain boundary degradation in LSM-YSZ composite Solid Oxide Fuel Cell cathodes operated in humidified air.* Journal of Power Sources, 2019. 438: p. 227043.
86. Hardy, J.S., et al., *Evaluation of cation migration in lanthanum strontium cobalt ferrite solid oxide fuel cell cathodes* via *in-operando X-ray diffraction.* Journal of Materials Chemistry A, 2018. 6(4): p. 1787-1801.
87. Wang, R., et al., *Comparison of chromium poisoning between lanthanum strontium manganite and lanthanum strontium ferrite composite cathodes in solid oxide fuel cells.* Journal of Power Sources, 2020. 476: p. 228743.
88. Egger, A., et al., *Effect of Microstructure on the Degradation of La0.6Sr0.4CoO3-δ electrodes in dry and humid Atmosphere.* Fuel cells, 2019.
89. Wang, J., et al., *Effect of humidity on La0.4Sr0.6Co0.2Fe0.7Nb0.1O3−δ cathode of solid oxide fuel cells.* International Journal of Hydrogen Energy, 2018. 44.
90. Hagen, A., K. Neufeld, and Y.-l.J.J.o.T.E.S. Liu, *Effect of Humidity in Air on Performance and Long-Term Durability of SOFCs.* 2010. 157.

 doi:10.20944/preprints202405.0747.v1